

RSC Advances



This is an *Accepted Manuscript*, which has been through the Royal Society of Chemistry peer review process and has been accepted for publication.

Accepted Manuscripts are published online shortly after acceptance, before technical editing, formatting and proof reading. Using this free service, authors can make their results available to the community, in citable form, before we publish the edited article. This *Accepted Manuscript* will be replaced by the edited, formatted and paginated article as soon as this is available.

You can find more information about *Accepted Manuscripts* in the [Information for Authors](#).

Please note that technical editing may introduce minor changes to the text and/or graphics, which may alter content. The journal's standard [Terms & Conditions](#) and the [Ethical guidelines](#) still apply. In no event shall the Royal Society of Chemistry be held responsible for any errors or omissions in this *Accepted Manuscript* or any consequences arising from the use of any information it contains.

1 *Preparation and characterization of photoactive antimicrobial graphitic carbon*
2 *nitride (g-C₃N₄) films.*

3 *John H. Thurston^{a,*}, Necia M. Hunter^a, Kenneth A. Cornell^b*

4 ^aDepartment of Chemistry, The College of Idaho, 2112 Cleveland Blvd, Caldwell, ID 83605

5 ^bDepartment of Chemistry and Biochemistry, Boise State University, Boise, ID 83725

6 **Abstract**

7 Photoactive films derived from nanostructured samples of the metal-free, intermediate
8 band gap semiconductor graphitic carbon nitride (ns-g-C₃N₄) have been synthesized and
9 characterized for their particle properties and antimicrobial activity. Physical characterization
10 reveals that these materials are composed of discrete nanoparticles whose dimensions range from
11 200 nm to 700 nm. Investigation of the photochemical reactivity of ns-g-C₃N₄ using coumarin-
12 3-carboxylic acid (3-CCA) indicates that this material produces reactive oxygen species (ROS)
13 under visible radiation. When irradiated with 0.31J visible light, ns-g-C₃N₄-based materials
14 reduced the viability of both gram-negative *Escherichia coli* O157:H7 and gram-positive
15 *Staphylococcus aureus* by approximately 50%. Nearly complete inactivation of both strains of
16 microorganisms was achieved upon administration of a 0.62J dose of visible radiation.
17 Importantly, no biocidal activity was observed for non-irradiated samples, indicating that the g-
18 C₃N₄-derived films are not inherently toxic in the absence of visible light. The results of this
19 study suggest that materials and, by extension, films and coatings derived from g-C₃N₄ may
20 present a novel route for controlling pathogenic microorganisms on surfaces in the environment,
21 and could be useful in reducing incidents of hospital-acquired infections.

22 Introduction

23 The acquisition of antibiotic-sensitive and antibiotic-resistant nosocomial infections are
24 correlated with an overall increase in patient morbidity and mortality, and responsible for annual
25 treatment costs of approximately \$9.8 billion.¹ It is estimated that there are 440,000 cases of
26 drug-resistant nosocomial infections among the U.S. adult population each year.¹

27 Of particular concern in hospital-acquired infections is the potential of solid surfaces to serve
28 as reservoirs of pathogenic microorganisms. This is particularly true for surfaces with high touch
29 frequencies, such as door handles, bed rails, and toilet seats.² A variety of gram-positive
30 bacteria, including vancomycin-resistant *Enterococcus* (VRE) and methicillin-resistant *S. aureus*
31 (MRSA), have been reported to survive for months on dry surfaces.³ The same study reported
32 that gram-negative species (*E. coli*, *Klebsiella* spp.) and the fungal pathogen *Candida albicans*
33 also survived on dry surfaces for extended periods of time.³ Similarly, wet surfaces, including
34 bedding, ultrasonic nebulizers and ventilation grills have been observed to function as
35 environmental reservoirs for MRSA.²

36 The mechanism by which environmental reservoirs facilitate microbial transmission in a
37 hospital setting remains the subject of much study.⁴ In the case of VRE, it has been reported that
38 touching a contaminated surface can result in microbial transfer with approximately the same
39 frequency as contact with a colonized patient.⁴ Reports have also shown that environmental
40 decontamination is able to successfully suppress outbreaks of MRSA and VRE.⁴ Consequently,
41 there is a clear incentive to develop new technologies for surface decontamination to reduce the
42 incidence of hospital-acquired infections or biofilm formation.

43 A wide variety of materials, including wide band gap semiconductors^{5, 6}, silver-based
44 materials⁷, antimicrobial polymers⁸ and biopolymers⁹⁻¹¹, carbon nanotubes^{12, 13} and

45 functionalized clays^{5, 14} have been used to produce novel antimicrobial coatings. Among these
46 technologies, narrow or intermediate band gap semiconductors that photo-catalytically generate
47 cytotoxic reactive oxygen species (ROS) from molecular oxygen show particular promise for the
48 reduction of bacterial populations in interior environments.^{15, 16} Graphitic carbon nitride (*g*-
49 C₃N₄) is an emerging metal-free, intermediate band gap semiconductor.¹⁷⁻²⁰ This material is
50 particularly attractive for environmental remediation applications due to the fact that *g*-C₃N₄
51 based materials have been shown to produce a variety of ROS in solution²¹⁻²⁵, are resistant to
52 photo-bleaching, and are stable under repeated electronic cycling while also being photo-
53 responsive to visible wavelengths of electromagnetic radiation.²⁴

54 The potential biocidal or antimicrobial utility of *g*-C₃N₄ is poorly explored. Two studies have
55 described the antimicrobial properties of composite *g*-C₃N₄ complexes containing either
56 monoclinic sulfur or Ag₂CO₃.^{26, 27} Two additional studies detail the ability of *g*-C₃N₄ to
57 promote the solution-state disinfection of single strains of microorganisms.^{28, 29} However, all of
58 these reports have relied on aqueous suspensions of the *g*-C₃N₄ materials to achieve the reported
59 antimicrobial effects. Surprisingly, there have been no studies exploring the utility of *g*-C₃N₄ for
60 the fabrication of biocidal surfaces or surface coverings or coatings, an application for which this
61 material appears to be uniquely suited. In addition, the ability of *g*-C₃N₄ to exhibit demonstrable
62 activity against both gram-positive and gram-negative microorganisms has yet to be established.
63 Herein we describe the synthesis and physical characterization of nanostructured samples of *g*-
64 C₃N₄ as well as the results of studies demonstrating visible-light driven antimicrobial activity of
65 *g*-C₃N₄-derived films against the clinically relevant microbes *S. aureus* and *E. coli* O157:H7.

66

67 **Experimental**

68 Reagents. All chemicals and media components were either purchased from Sigma-Aldrich
69 Corp. (St. Louis, MO) or from Fisher Scientific (Pittsburgh, PA). Pure strain samples of *E. coli*
70 O157:H7 (ATCC #43894) and *S. aureus* (ATCC #6538) were purchased from the ATCC
71 (Mannassas, VA) and were grown using Luria Bertani (LB) broth or agar.

72 Preparation of $g\text{-C}_3\text{N}_4$: Samples of $g\text{-C}_3\text{N}_4$ were prepared by a slight modification of the
73 reported procedures.^{22, 24, 30} Briefly, 2.0 g of dicyandiamide was placed in a porcelain crucible
74 and heated from 25°C to 575°C at a rate of 175°C/hour in a muffle furnace. The sample dwelled
75 at 575°C for four hours and then was cooled to ambient temperature over 18 hours. The
76 resulting yellow solid was ground to free flowing powder in an agate mortar and pestle prior to
77 analysis and additional modification.

78 Preparation of nanostructured $g\text{-C}_3\text{N}_4$: Samples of nanostructured $g\text{-C}_3\text{N}_4$ (ns- $g\text{-C}_3\text{N}_4$) were
79 prepared using a modification of the protocol reported by Yang *et al.*³¹ A 200mg portion of bulk
80 $g\text{-C}_3\text{N}_4$ powder was suspended in 20 mL of 2-propanol and the resulting mixture was subjected
81 to sonication at room temperature for 24 hours. After 24 hours, 20 mL of 0.9% saline solution
82 was added to the mixture and the alcoholic solvent removed *via* azeotropic distillation to produce
83 a 10 mg/mL aqueous suspension of nanostructured $g\text{-C}_3\text{N}_4$.

84 Spectroscopic characterization of $g\text{-C}_3\text{N}_4$ and ns- $g\text{-C}_3\text{N}_4$: Infrared spectra were collected on a
85 Thermo-Nicolet Avatar 360 FT-IR spectrophotometer equipped with a single reflection Smart
86 Orbit diamond ATR aperture in the range of 4000 – 400 cm^{-1} . Fluorescence spectra were
87 collected on a Varian Cary Eclipse Fluorescence spectrophotometer. Diffuse reflectance UV-Vis
88 spectroscopy measurements were collected on powder samples using a Cary 5000
89 spectrophotometer. Bandgap values are estimated using Kubelka-Munk theory.^{32, 33} Raman data

90 was collected on a Thermo Nicolet 870 instrument that was coupled to an FT-Raman module.
91 X-ray photoelectron spectroscopy was conducted on a PHI 5000 Versaprobe II Scanning ESCA
92 microprobe using a monochromatic Al K_{α} X-ray source (1486.6 eV). The base vacuum in the
93 chamber was better than 1.5×10^{-10} torr. The samples used in this study were probed by an X-
94 ray source with a power of 100W and a beam diameter of 150 μ m. Survey scans were collected
95 on several different areas to study the relative composition of the sample. High resolutions scans
96 were performed on each elemental region to improve the signal-to-noise ratio. Sample charging
97 effects were minimized using a low energy electron gun and Ar^{+} ions. The binding energy scale
98 was referenced to the C1s peak (284.8 eV) to accommodate peak shifts as a consequence of
99 sample charging effects.

100 Physical characterization of $g-C_3N_4$ and ns- $g-C_3N_4$: Secondary electron images of $g-C_3N_4$ and
101 ns- $g-C_3N_4$ were recorded on a Hitachi S-3400N analytical scanning electron microscope
102 operating at an accelerating potential of 10.0 kV. Samples were prepared by dispersing the
103 powder on adhesive carbon tapes and sputter coating with chromium to prevent charging and to
104 increase contrast. The hydrodynamic radius of the materials developed for this study was
105 measured using dynamic light scattering (DLS) measurements on a Zetasizer Nano ZS
106 Zetapotential/Particle size analyzer (Malvern Instruments) equipped with a monochromatic and
107 coherent light beam (633 nm He-Ne laser, 4 mW). Powdered samples of $g-C_3N_4$ or ns- $g-C_3N_4$
108 were dispersed in deionized water to get a pre-determined concentration of 0.001 wt% aqueous
109 solution. The samples used for analysis were subjected to ultrasonication for about 10 mins and
110 immediately transferred to zeta cell for measurements. The particle size scans were averaged to
111 obtain size distribution data. Powder x-ray diffraction data was collected on a Rigaku Miniflex

112 600 powder x-ray diffractometer using Cu K_{α} radiation (graphite monochromator, $\lambda = 1.5418$
113 Å). Data was collected between 2.0° and 65.0° on 2θ with a step size of 0.01° .

114 Irradiation procedures: Irradiation experiments were carried out by illuminating the sample
115 mixture with an ozone free xenon light source operating at 270 W (Power source: Newport #
116 69911). The lamp housing (Newport # 67001) contained an F/2.2 fused silica condenser and rear
117 reflector (1.6 correction factor). The photon flux was stripped of infra-red radiation using a
118 temperature-controlled, recirculating water filter. Similarly, UV radiation was removed using a
119 $\lambda = 400$ nm cut-off filter (Oriel # FSQ-GG400). Total radiation doses were estimated using an
120 average source irradiance of $30 \text{ mW}\cdot\text{m}^{-2}\cdot\text{nm}^{-1}$ (working distance = 0.5 m), a collimated beam
121 diameter of 33 mm, and applying equations 1-3.

122

$$\text{Radiant Exitance (W}\cdot\text{m}^{-2})=M_e=1.6\times 0.05\times \frac{30\text{mW}}{\text{m}^2\cdot\text{nm}} \int_{\lambda_1}^{\lambda_2} d\lambda \quad \text{Equation 1}$$

$$\text{Radiant Power (W)}=\varphi_e=A\times M_e \quad \text{Equation 2}$$

$$\text{Total Radiant Dose (J)}=\text{Radiant Energy (J)}= \varphi_e\times t \quad \text{Equation 3}$$

123

124 The variables A and t represent the incident beam area (m^2) and irradiation time (s), respectively.
125 Only incident radiation whose wavelengths fell in the spectral window between the UV cutoff
126 filter ($\lambda_1 = 400$ nm) and the experimentally determined band gap of the semiconductor ($\lambda_2 = 442$
127 nm) were used in the dose calculations.

128 Determination of ROS production: A 200mg sample of ns-g- C_3N_4 was suspended in 20 mL 2
129 mM coumarin-3-carboxylic acid in 0.9% saline.³⁴ The sample was stirred at 260 rpm and the
130 mixture was either covered (dark control) or subjected to visible radiation. Aliquots of the

131 reaction mixture and dark control were collected prior to the start of irradiation ($t = 0$) and
132 periodically throughout the experiment ($t = 1, 2, 4$ hr). The photocatalyst was removed from the
133 reaction mixture by centrifugation at $10,000 \times g$ for 10 minutes and passage through a syringe
134 filter ($0.2 \mu\text{m}$). The fluorescence intensity of the resulting solution was measured at 450 nm
135 using an excitation wavelength of 395 nm (1.5nm slit) and an emission scan of 400-500 nm.

136 Antimicrobial experiments: Several isolated colonies of either *E. coli* O157:H7 or *S. aureus*
137 cultures grown overnight on LB agar were suspended in 5 mL 0.9% sterile saline. The volume
138 of the suspension was adjusted to bring the final absorbance (600 nm) to 0.5. The resulting
139 solution was serially diluted to 10^{-6} using ice-cold sterile saline.³⁵ A 1.0 mL portion of the 10^{-6}
140 dilution was combined with 20 mL of sterile 0.9% saline containing 20 mg ns-g-C₃N₄ and the
141 resulting mixture vacuum filtered onto a $0.45 \mu\text{m}$ nitrocellulose filter disk (47 mm disk
142 diameter). These experimental conditions resulted in a bacterial loading densities of ~ 11.4
143 CFU/cm² (*E. coli* O157:H7) and ~ 14.4 CFU/cm² (*S. aureus*). In all cases, the microbial loading
144 density was selected to be 4-5 times higher than the average density of MRSA reported to be
145 present on elevated surfaces in a hospital environment (~ 3.5 CFU/cm²).³⁶ To measure
146 nonspecific cytotoxicity (*e.g.* heating effects), replicate filters were prepared that contained
147 bacteria, but lacked ns-g-C₃N₄.

148 Prior to irradiation, inoculated nitrocellulose filter disks were placed on pieces of sterile saline-
149 dampened Whatman #1 filters in a glass petri dish. The filters were irradiated for 0, 30, 60, or
150 120 minutes ($\sim 0-0.68$ J applied radiation). Controls consisted of similarly prepared filters that
151 received no irradiation (dark control), or similarly irradiated/non-irradiated inoculated filters
152 lacking ns-g-C₃N₄. The glass petri dish was placed on ice during the irradiation to minimize cell
153 killing due to direct sample heating. After irradiation, the nitrocellulose filter disk was placed on

154 LB agar and incubated for 24 hrs at 37°C. After the incubation period, colony forming units
155 (CFU) on the disk were counted manually, and the % total CFU calculated using the formula:

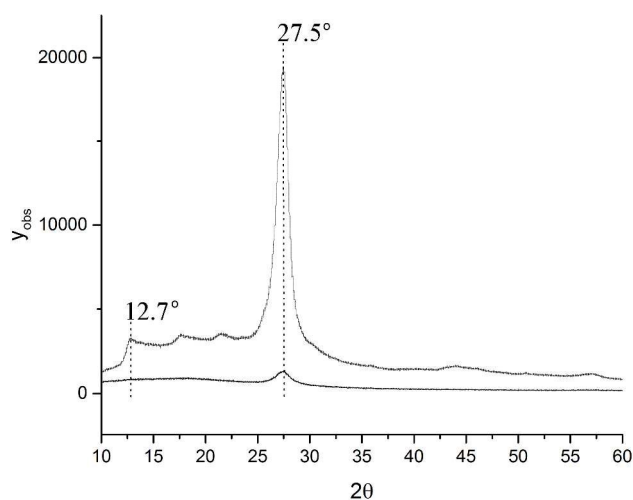
$$156 \quad \% \text{ Total CFU} = \frac{\text{Test CFU}}{\text{Total CFU (t=0)}} \times 100 \quad \text{Equation 4}$$

157 Each experiment was performed three times, with each time point tested in triplicate. The results
158 of the experiments are expressed as the mean % total CFU \pm SEM (standard error on the mean).
159 In all cases, the experiments were stopped when the colony count dropped below 2.5 CFU/cm²,
160 an accepted threshold for the decontamination of high touch frequency sites.³⁷

161 **Results and Discussion**

162 Preparation of ns-g-C₃N₄

163 Bulk samples of g-C₃N₄ were prepared by direct thermal polymerization of the molecular
164 precursor dicyandiamide in a manner similar to procedures described elsewhere.³⁰ The
165 successful formation of the desired graphitic phase of carbon nitride was confirmed by powder
166 X-ray diffraction experiments (Figure 1). In particular, the peak at $2\theta = 27.5^\circ$ corresponds to the
167 interlayer spacing ($d = 3.24\text{\AA}$) for g-C₃N₄, while a second peak observed at $2\theta = 12.7^\circ$ closely
168 matches the dimensions expected for the spacing of the individual melon subunits present in the
169 polymeric material ($d = 6.94\text{\AA}$).



170

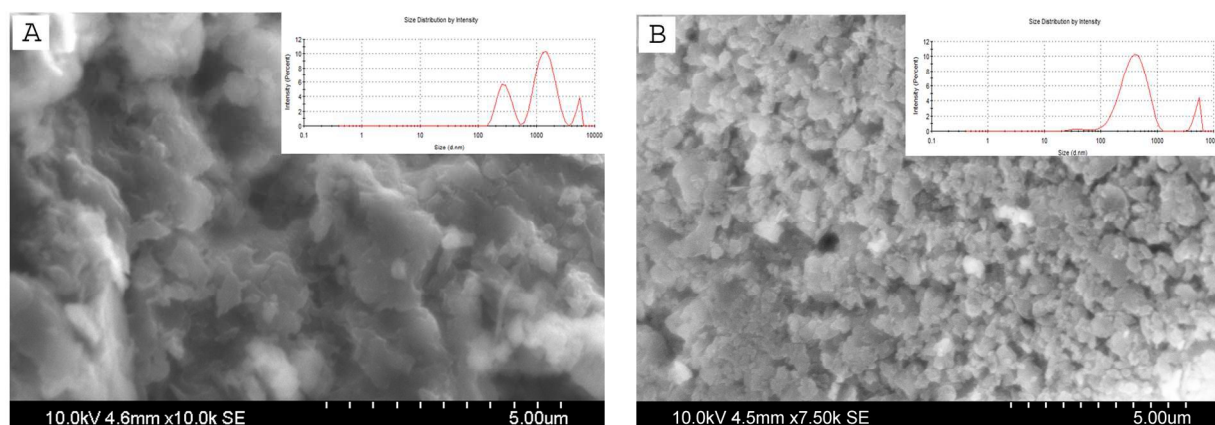
171 **Figure 1:** Powder X-ray diffraction data for samples of $g\text{-C}_3\text{N}_4$ (top trace) and $ns\text{-}g\text{-C}_3\text{N}_4$
172 (bottom trace). Peaks observed at $2\theta = 27.5^\circ$ and 12.7° are consistent with interlayer spacing and
173 individual melon subunit spacing, respectively, for the material.

174

175 Post-synthesis modification of $g\text{-C}_3\text{N}_4$ using either physical or chemical techniques has been
176 previously reported to produce nanostructured samples of the material ($ns\text{-}g\text{-C}_3\text{N}_4$).³¹ As part of
177 this study, we have explored the formation of antimicrobial films from $ns\text{-}g\text{-C}_3\text{N}_4$ on the basis of
178 two principle considerations: First, the reduced particle size is anticipated to facilitate the
179 formation of materials with an overall improved degree of structural homogeneity. Second, the
180 smaller particle size present in the exfoliated samples will favor charge carrier migration to the
181 semiconductor surface over deleterious recombination events.¹⁵ This, in turn, is anticipated to
182 result in enhanced photochemical activity and quantum efficiency of these systems, with respect
183 to the desired antimicrobial applications.

184 Samples of $ns\text{-}g\text{-C}_3\text{N}_4$ used in this study were produced by means of a sonication-induced
185 exfoliation process. The effects of exfoliation on the structure and morphology of $g\text{-C}_3\text{N}_4$ were
186 investigated by powder X-ray diffraction and scanning electron microscopy, and the

187 hydrodynamic radius of the materials before and after the sonication process were compared. As
188 shown in Figure 1, the strong reflection centered at $2\theta = 27.5^\circ$ arising from the interlayer spacing
189 of the bulk material is also observed in samples of ns- $g\text{-C}_3\text{N}_4$, indicating that the lamellar
190 structure of the material is conserved through the exfoliation process. Investigation of the
191 morphology of the materials by scanning electron microscopy revealed that bulk $g\text{-C}_3\text{N}_4$ consists
192 principally of large, extended layers (Figure 2-A). In contrast, as illustrated in Figure 2-B,
193 samples that have been subjected to sonication are observed to be composed of discrete particles
194 with dimensions ranging from approximately 200 - 700 nm. The results of the electron
195 microscopy analysis correlate well with the experimentally measured hydrodynamic radius of
196 samples of the bulk and exfoliated $g\text{-C}_3\text{N}_4$. Bulk $g\text{-C}_3\text{N}_4$ consisted of approximately 66.7%
197 particles with dimensions of $1.48 \pm 0.51 \mu\text{m}$ (inset Figure 2-A). In contrast, analysis of ns- $g\text{-C}_3\text{N}_4$
198 revealed that 90% of the samples were composed of particles with dimensions of 419 ± 198
199 nm (inset Figure 2-B).

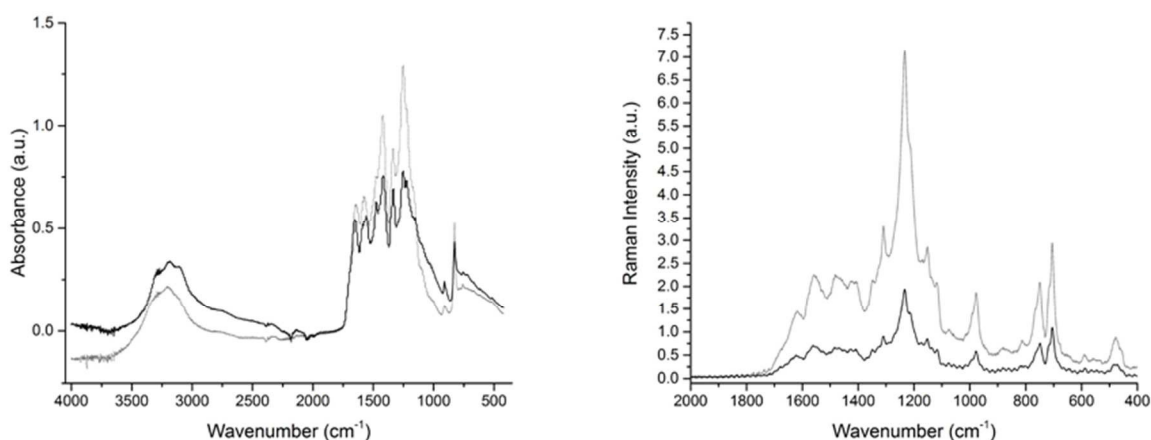


200

201 **Figure 2:** Scanning electron micrographs detailing the morphology of samples of (A) $g\text{-C}_3\text{N}_4$
202 (10.0k magnification) and (B) ns- $g\text{-C}_3\text{N}_4$ (7.50k magnification) produced through sonication
203 induced exfoliation of the bulk material in 2-propanol. Inset images detail the relative particle
204 size distribution as observed through hydrodynamic radius measurements.

205 The chemical composition of the ns- $g\text{-C}_3\text{N}_4$ was investigated by absorbance spectroscopy (FT-
206 IR and Raman) and x-ray photoelectron spectroscopy (XPS). The FT-IR spectrum of both the

207 bulk $g\text{-C}_3\text{N}_4$ and exfoliated $ns\text{-}g\text{-C}_3\text{N}_4$ demonstrated the characteristic vibrational and breathing
208 modes associated with the heptazine subunits and the terminal amine functional groups present
209 in the extended structure of $g\text{-C}_3\text{N}_4$ (Figure 3, *left*). The sharp absorbance observed at 808 cm^{-1}
210 may originate from either $s\text{-triazine}$ or from heptazine ring units, while the numerous peaks
211 found between 900 cm^{-1} and 1800 cm^{-1} are in excellent agreement with reported data for samples
212 of $g\text{-C}_3\text{N}_4$ produced *via* thermal polymerization reactions.^{22, 38} One notable exception is the
213 strong absorbance peak observed at 1402 cm^{-1} . This peak has previously been attributed to the
214 presence of $s\text{-triazine}$ (C_3N_3) in the material, which suggests that the initial bulk materials were
215 incompletely condensed.³⁹ It is notable that the relative intensity of the absorbance peak at 1402
216 cm^{-1} decreases significantly in the exfoliated samples, suggesting that the sonication employed in
217 the fabrication of the $ns\text{-}g\text{-C}_3\text{N}_4$ promotes additional aggregation and condensation of residual $s\text{-}$
218 triazine units that were present in the bulk material.



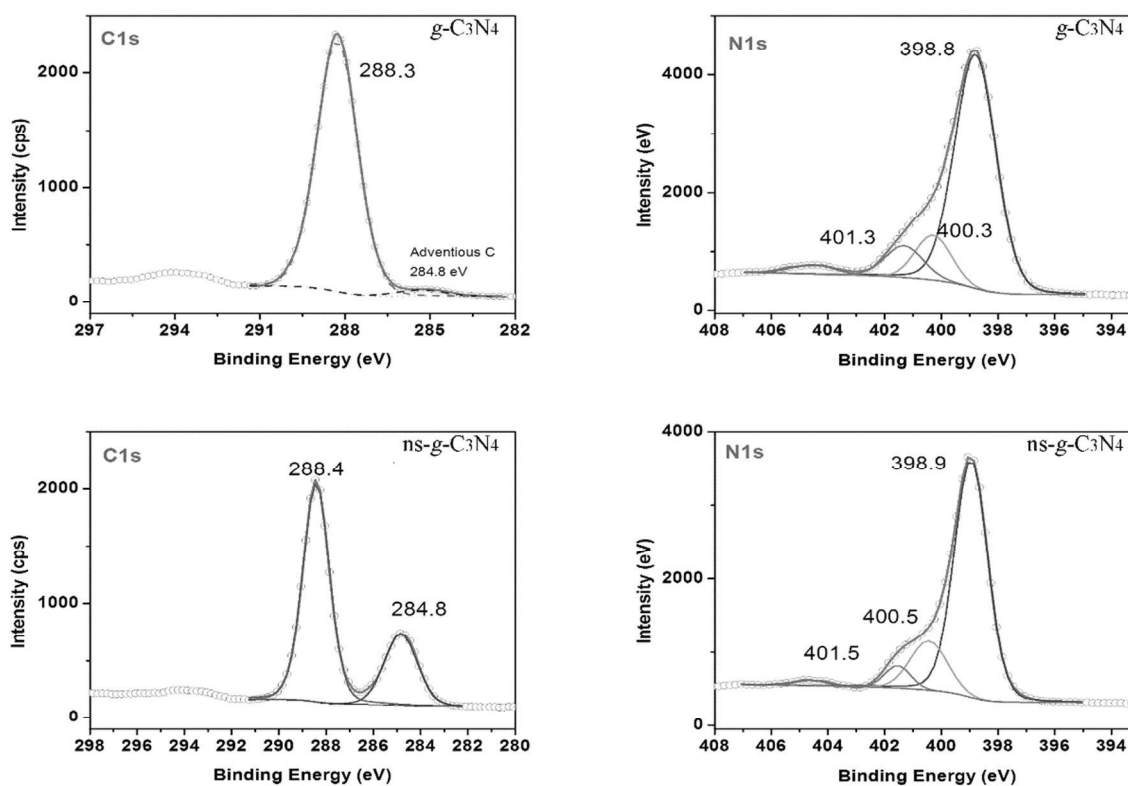
219

220 **Figure 3:** Fourier transform infrared (FTIR) absorbance spectrum (left) and Raman spectrum
221 (right) of $g\text{-C}_3\text{N}_4$ produced via thermal polymerization of dicyandiamide (grey) and $ns\text{-}g\text{-C}_3\text{N}_4$
222 produced via sonication induced exfoliation of the bulk material (black). The spectra reveal a
223 general conservation of structure and composition in forming $ns\text{-}g\text{-C}_3\text{N}_4$ from $g\text{-C}_3\text{N}_4$.
224

225 The results of the FT-IR experiments are supported by Raman spectroscopy (Figure 3, *right*).
226 Raman spectroscopy has been widely used to assess the internal structure of carbon-based
227 materials.⁴⁰ In this case, the peak at approximately 1600cm^{-1} (*G* mode) can be attributed to
228 vibrations arising from sp^2 hybridized carbon atoms. In contrast, the peak at 1350cm^{-1} (*D* mode)
229 is a product of vibrations arising from sp^3 hybridized carbon centers.³⁹ These sp^3 hybridized
230 carbon centers are not associated with the accepted structure of $g\text{-C}_3\text{N}_4$ and can be viewed as
231 defects in the lamellar structure of the complex. Consequently, the ratio of the Raman peak
232 intensity (I_D/I_G) can serve as a measure of the evolution of the relative structural disorder in the
233 material as a consequence of the initial polymerization and subsequent exfoliation process. In
234 this case, the I_D/I_G ratio for the bulk material was calculated to be 1.66, whereas the I_D/I_G ratio
235 for the exfoliated samples of $\text{ns-}g\text{-C}_3\text{N}_4$ was 1.42. These ratios support the results of the FT-IR
236 analysis and suggest that samples of $\text{ns-}g\text{-C}_3\text{N}_4$ have a smaller number of interstitial defects
237 relative to the bulk materials. These results are consistent with an exfoliation-and-regrowth
238 mechanism that has previously been proposed for the formation of nanostructured $g\text{-C}_3\text{N}_4$
239 materials.³⁹

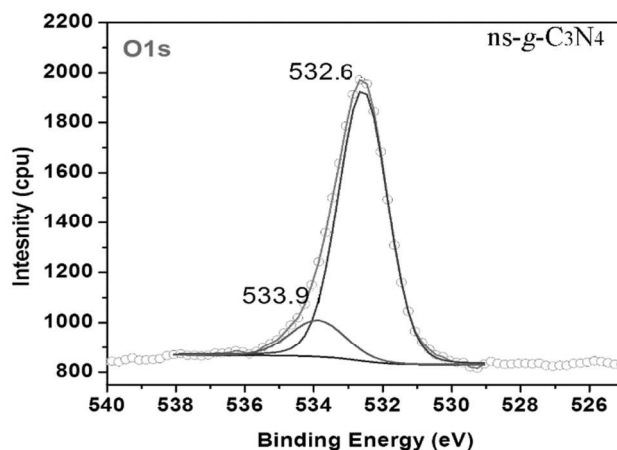
240 The effects of the sonication process on the composition of the $g\text{-C}_3\text{N}_4$ samples were
241 investigated by X-ray photoelectron spectroscopy (XPS). In particular, we sought to confirm
242 that the formation of $\text{ns-}g\text{-C}_3\text{N}_4$ did not fundamentally alter the chemical composition of the
243 material or introduce additional functional groups that could negatively impact the biological
244 compatibility of the materials. As illustrated in Figure 4, bulk samples of $g\text{-C}_3\text{N}_4$ contain a single
245 significant carbon environment with a binding energy of 288.3 eV. This peak is consistent with
246 sp^2 hybridized carbon centers in nitrogen-containing aromatic rings (N-C=N). This peak is
247 effectively unchanged in the nanostructured sample (288.4 eV). A second, significant peak

248 correlating to adventitious graphitic carbon contamination (sp^2 C-C) is also observed in samples
 249 of ns- g - C_3N_4 . This peak may be observed as a consequence of the solution-based synthetic
 250 methodology employed in the fabrication of these materials as part of this study. The N 1s
 251 spectrum of bulk and ns- g - C_3N_4 has been resolved into three components with binding energies
 252 of 398.8 eV (sp^2 C=N-C), 400.3 eV (N(3)) and 401.3 eV (conjugated N-H chemical
 253 environment), respectively. The relative intensity of the N-H peak decreases in moving from the
 254 bulk to the nanostructured material, while the intensity of the N(3) peak simultaneously
 255 increases. This data further reinforces the FT-IR results, suggesting that sonication of bulk g -
 256 C_3N_4 facilitates additional condensation and internal organization of the extended material.



257
 258 **Figure 4:** High resolution X-ray photoelectron spectra of g - C_3N_4 (top) and ns- g - C_3N_4 (bottom)
 259 samples of that were employed in this study. In both cases, the identified peaks are consistent
 260 with the chemical environments anticipated to be present in the layered carbon nitride structure.
 261

262 The XPS spectra failed to show significant evidence of oxygen in the bulk samples of $g\text{-C}_3\text{N}_4$.
263 Oxygen was detected in the nanostructured materials and the resulting O1s spectrum was de-
264 convoluted into two peaks with binding energies of 532.6 eV and 533.9 eV. The 532.6 eV peak
265 likely corresponds to surface hydroxyl groups of the silicon sample holder, while the 533.9 eV
266 peak corresponds to chemisorbed water molecules on the surface of the ns- $g\text{-C}_3\text{N}_4$ sample.⁴¹
267 Importantly, the XPS spectrum of ns- $g\text{-C}_3\text{N}_4$ contains no evidence for either C-O or C=O species
268 that would indicate partial oxidation of the $g\text{-C}_3\text{N}_4$ precursor.



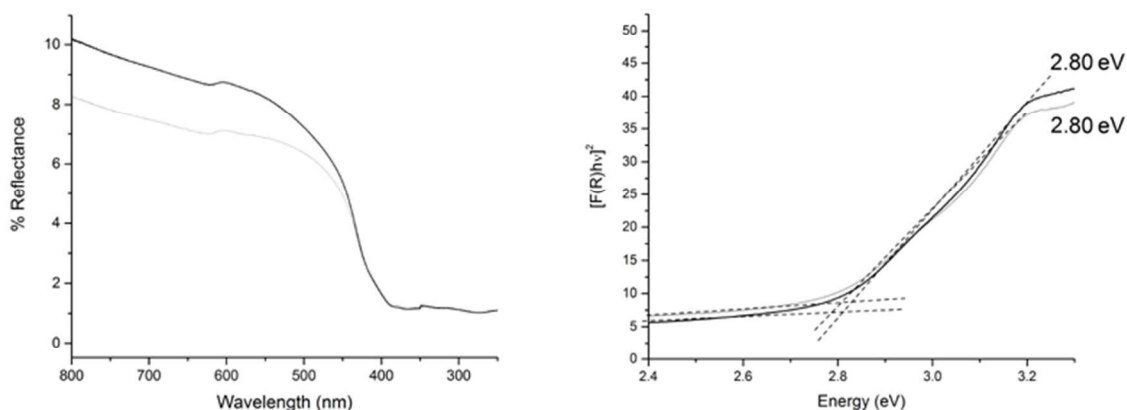
269

270 **Figure 5:** High resolution O1s X-ray photoelectron spectrum of bulk ns- $g\text{-C}_3\text{N}_4$.

271

272 Optical and Photochemical Properties of ns- $g\text{-C}_3\text{N}_4$

273 Samples of $g\text{-C}_3\text{N}_4$ are established intermediate band gap semiconductors.^{42, 43} As determined
274 by diffuse reflectance spectroscopy, the bulk and exfoliated samples of $g\text{-C}_3\text{N}_4$ both possess
275 measured band gap energies of approximately 2.80 eV (Figure 6, *right*). The similarity in the
276 optical properties of the materials reinforces the results of the XPS studies (Figure 4) and further
277 indicates that no significant change in the chemical composition of the material occurred during
278 the process of exfoliation.



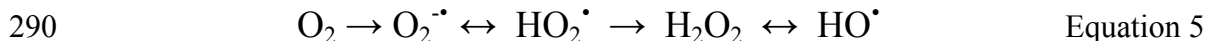
279

280 **Figure 6:** Diffuse reflectance UV-Vis spectrum (left) and calculated band gap energies (right) of
 281 samples of *g*-C₃N₄ (grey trace) and *ns-g*-C₃N₄ (black trace).
 282

283 With respect to antimicrobial applications, the ability of a semiconductor to produce ROS is of
 284 fundamental importance.⁴⁴ The superoxide radical anion is likely the initial species that will be
 285 produced from the photochemical reduction of molecular oxygen.⁴⁵ This complex is highly
 286 reactive in aqueous solution and produces a number of additional ROS, including hydrogen
 287 peroxide (H₂O₂), the hydrogen peroxy radical (HO₂[•]) and hydroxyl radical (HO[•]) (Equation 5).

288 ¹⁵

289



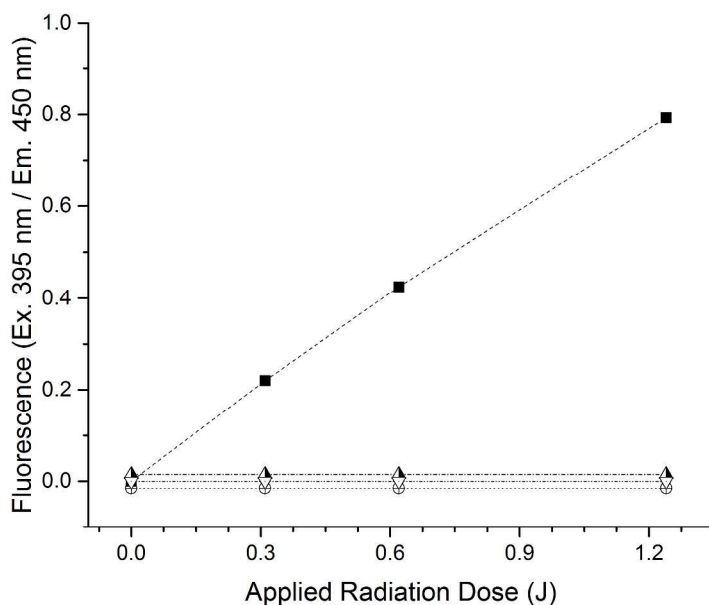
291

292 All ROS cause significant damage to cellular components of microorganisms and are
 293 potentially cytotoxic.⁴⁶ While it is clear that *g*-C₃N₄ does not contain the ionic bonding that
 294 typifies many traditional semiconducting materials, it is reported that the reduction potential of
 295 the conduction band of *g*-C₃N₄ can be estimated using Equation 6:³⁸

$$296 \quad E_{CB}^0 = X - E^C - \frac{1}{2}E_g \quad \text{Equation 6}$$

297 In this case, X is the geometric mean of the electronegativity of the constituent atoms of the
298 semiconductor material (calculated to be 4.73 eV^{47} for $g\text{-C}_3\text{N}_4$), E^C is a scaling factor that relates
299 the absolute vacuum scale to the normal hydrogen scale ($\sim 4.5 \text{ eV}$), and E_g is the experimentally
300 determined band gap energy of the material. The calculated conduction band and valence band
301 edge potentials for $ns\text{-}g\text{-C}_3\text{N}_4$ are -1.17 V and 1.63 V , respectively. The conduction band edge
302 reduction potential of $ns\text{-}g\text{-C}_3\text{N}_4$ is more negative than both the standard redox potential of
303 molecular oxygen ($\text{O}_2/\text{O}_2^{\cdot-}$, $E^\circ = -0.33 \text{ V}$) and the redox potential of a 1 M aqueous solution of
304 dioxygen ($\text{O}_2/\text{O}_2^{\cdot-}$, $E^\circ = -0.16 \text{ V}$).⁴⁵ Consequently, it is possible to conclude that the materials
305 used in this study have sufficient reducing power to promote the photochemical conversion of
306 surface adsorbed oxygen molecules into ROS under appropriate experimental conditions.

307 We have confirmed the photochemical behavior of $ns\text{-}g\text{-C}_3\text{N}_4$ using the established, selective
308 hydroxyl radical scavenging molecule coumarin-3-carboxylic acid (3-CCA).⁴⁸ In solution,
309 reaction of 3-CCA with hydroxyl radicals produces the highly fluorescent molecule 7-
310 hydroxycoumarin-3-carboxylic acid. As illustrated in Figure 7, irradiated reaction mixtures of
311 $ns\text{-}g\text{-C}_3\text{N}_4$ and 3-CCA produced 7-hydroxycoumarin-3-carboxylic acid and a concomitant
312 increase in fluorescence. In contrast, non-irradiated sample mixtures, or irradiated samples
313 containing only $ns\text{-}g\text{-C}_3\text{N}_4$ or only 3-CCA, showed no observable change in the fluorescence.
314 While direct oxidation of 3-CCA is theoretically possible, we anticipate that the Cl^- present in the
315 reaction mixture will serve to trap the photogenerated holes and favor ROS production by means
316 of reduction of surface adsorbed dioxygen.⁴⁹ These results indicate that $ns\text{-}g\text{-C}_3\text{N}_4$ successfully
317 reduced molecular oxygen to produce cytotoxic ROS in the presence of visible radiation.

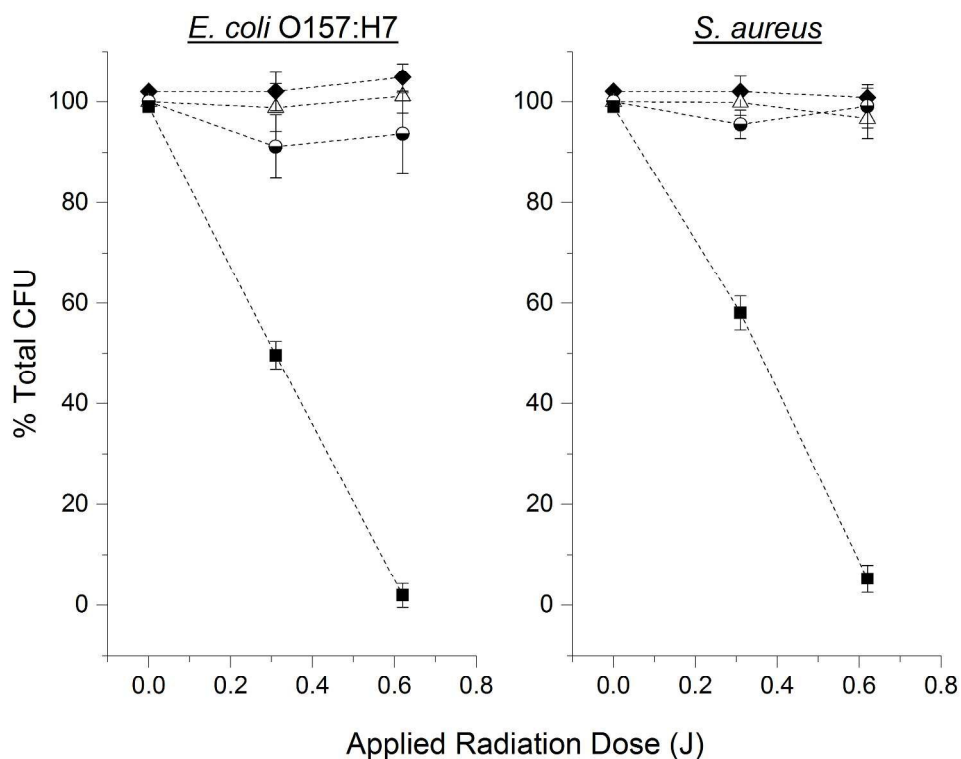


318

319 **Figure 7:** Observed change in fluorescence ($\lambda_{\text{ex}} = 395 \text{ nm}$; $\lambda_{\text{em}} = 450 \text{ nm}$) in mixtures of 3-CCA
 320 and ns-g-C₃N₄ with (---■---) and without (---⊕---) irradiation with visible light ($400\text{nm} \leq \lambda \leq$
 321 442nm). Control reactions contained either irradiated 3-CCA alone (---▽---) or irradiated ns-g-
 322 C₃N₄ alone (---▲---).

323

324 Irradiated filters containing co-deposited samples of ns-g-C₃N₄ and either gram negative *E.*
 325 *coli* O157:H7 (Figure 8, *left*) or gram positive *S. aureus* (Figure 8, *right*) showed dramatic
 326 decreases in bacterial survivorship. In contrast, non-irradiated filters with co-deposited ns-g-
 327 C₃N₄ and bacterial cells (dark controls), and irradiated/non-irradiated filters containing only
 328 bacterial cells (no ns-g-C₃N₄) failed to impact bacterial survival. In the presence of ns-g-C₃N₄,
 329 irradiation with a 0.31J dose of visible light killed $49.4 \pm 2.8\%$ of *E. coli* O157:H7 cells, while a
 330 dose of 0.62J destroyed $97.1 \pm 2.4\%$ of the available CFUs (D-value = 112 min). Similarly, a
 331 total of $40.9 \pm 3.4\%$ of the available *S. aureus* CFUs were destroyed with a dose of 0.31J of
 332 visible radiation, while $93.7 \pm 2.7\%$ were eradicated with the 0.62J dose (D-value = 117 min).



333

334 **Figure 8:** Relative number of CFUs (■) of *E. coli* O157:H7 or *S. aureus* observed as a
335 function of applied radiation dose ($400\text{nm} \leq \lambda \leq 442\text{nm}$). Traces for dark control studies
336 conducted with (●) or without (◆) ns-*g*-C₃N₄, or irradiated without ns-*g*-C₃N₄ (△)
337 are also presented. Error bars represent the standard error of the mean for three independent
338 trials.

339

340 The results of the experiments described here indicate that the photoactive ns-*g*-C₃N₄ materials
341 are not inherently toxic, nor is the observed antimicrobial activity simply a product of
342 electromagnetic radiation-induced cellular damage.

343 The materials derived from *g*-C₃N₄ that are presented in this manuscript represent a specific
344 advance in the development of antimicrobial surface coatings. Primarily, we note that the *g*-
345 C₃N₄- films described in this study are photoresponsive to visible radiation. This stands in
346 contrast to the highly energetic UV radiation required to drive wide band gap photocatalysts such
347 as anatase TiO₂ and allows *g*-C₃N₄ to potentially function as antimicrobial and environmental

348 remediation agents in interior environments without the need for potentially damaging radiation
349 or cocatalysts.

350 Additionally, it is important to emphasize that the materials that we have developed in this
351 study are able to achieve comparable and, in some cases superior, results for surface disinfection
352 when challenged with either *E. coli* O157:H7 or *S. aureus*, relative to what has been reported for
353 other semiconducting antimicrobial surface coatings.⁵⁰⁻⁵³ The advantages of these *g*-C₃N₄-based
354 materials over other, previously reported systems are observed both in terms of the relative
355 required exposure time and in terms of the total reduction in CFU and are realized despite the
356 fact that higher energy, UV radiation was employed in many of the earlier disinfection studies.

357 The composition of the *g*-C₃N₄ films that were used in this study presents another specific
358 advantage. The lack of metals - especially copper and silver salts - in *g*-C₃N₄ is anticipated to
359 increase the overall biological compatibility of this material, while the extended, polymeric
360 structure may also act to suppress unwanted leaching and environmental redistribution. Lastly,
361 we note that the *g*-C₃N₄ polymer is readily prepared in large scale from inexpensive,
362 commercially available precursors. These properties suggest that films and coatings derived
363 from *g*-C₃N₄ may find application in a hospital environment for the decontamination of surfaces
364 with high touch frequency, including bed rails, countertops and door knobs, among others.

365 **Conclusion**

366 The intermediate band gap metal-free semiconductor ns-*g*-C₃N₄ was synthesized from bulk
367 samples of carbon nitride *via* a simple exfoliation procedure. Fluorescent studies using 3-CCA
368 indicate that irradiated samples of ns-*g*-C₃N₄ efficiently produce ROS. Films containing ns-*g*-
369 C₃N₄ material showed biocidal activity against both gram negative and gram positive bacteria
370 when exposed to visible radiation. Importantly, no antimicrobial activity was observed for ns-*g*-

371 C₃N₄-based films that were not exposed to visible radiation, indicating that the materials
372 developed for this study are not themselves inherently toxic. Ultimately, this work demonstrates
373 that photoactive ns-g-C₃N₄ is a promising candidate for a variety of biocidal and environmental
374 remediation applications.

375 **Corresponding Author**

376 *Author to be contacted for correspondence: email: jthurston@collegeofidaho.edu, phone:
377 (208)459-5531, fax: (208)459-5175

378 **Acknowledgements**

379 The work described in this publication was made possible by an Institutional Development
380 Award (IDeA) from the National Institute of General Medical Sciences of the National Institutes
381 of Health under Grants #P20GM103408 and #P20GM19095. We also acknowledge support from
382 The Biomolecular Research Center at Boise State with funding from the National Science
383 Foundation, Grants # 0619793 and #0923535; the MJ Murdock Charitable Trust; and the Idaho
384 State Board of Education.

385 The authors thank Dr. Madhu Kongara and Prof. Alex Punnoose at Boise State University for
386 help with the collection and analysis of the XPS and DRFTS data. Drs. Rick Ubrick and Karthik
387 Chinnathambi (Boise State Center for Materials Characterization) are gratefully acknowledged
388 for assistance with the collection and processing of electron microscopy and powder x-ray
389 diffraction data.

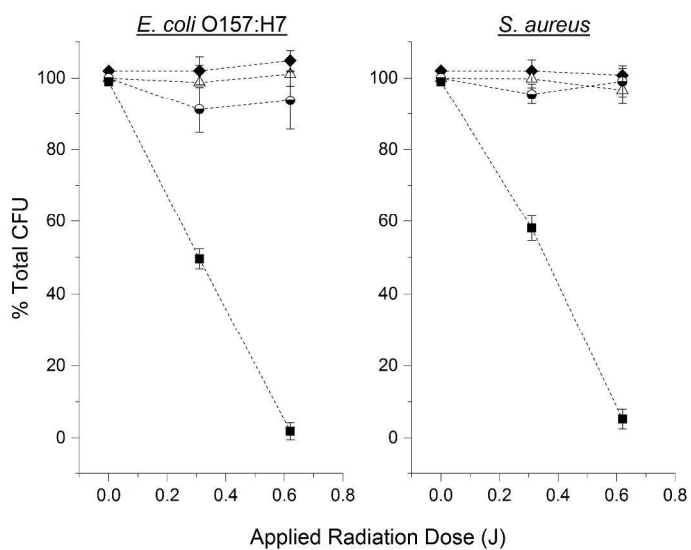
390 The contents of this manuscript are solely the responsibility of the authors and do not
391 necessarily represent the official views of NIH.

392

393 REFERENCES

- 394 1. E. Zimlichman, D. Henderson, O. Tamir, C. Franz, P. Song, C. K. Yamin, C. Keohane,
395 C. R. Denham and D. W. Bates, *JAMA Int. Med.*, 2013, **173**, 2039.
- 396 2. B. Hota, *Clin Infect Dis*, 2004, **39**, 1182-1189.
- 397 3. A. Kramer, I. Schwebke and G. Kampf, *BMC Infect. Dis.*, 2006, **6**, 130-130.
- 398 4. J. M. Boyce, *J. Hosp. Infect.*, 2007, **65**, Supplement 2, 50-54.
- 399 5. R. Dastjerdi and M. Montazer, *Colloid Surface B*, 2010, **79**, 5-18.
- 400 6. G. Fu, P. S. Vary and C.-T. Lin, *J. Phys. Chem. B*, 2005, **109**, 8889-8898.
- 401 7. M. Rai, A. Yadav and A. Gade, *Biotechnol. Adv.*, 2009, **27**, 76-83.
- 402 8. Y. Zhang, M. Ding, L. Zhou, H. Tan, J. Li, H. Xiao, J. Li and J. Snow, *Polym. Chem.*,
403 2012, **3**, 907-913.
- 404 9. E.-R. Kenawy, S. D. Worley and R. Broughton, *Biomacromolecules*, 2007, **8**, 1359-1384.
- 405 10. G. Ye, J. Lee, F. Perreault and M. Elimelech, *ACS Appl. Mater. Interfaces*, 2015, **7**,
406 23069-23079.
- 407 11. K. M. Xiu, Q. Cai, J. S. Li, X. P. Yang, W. T. Yang and F. J. Xu, *Colloid Surface B*,
408 2012, **90**, 177-183.
- 409 12. I. Banerjee, D. Mondal, J. Martin and R. S. Kane, *Langmuir*, 2010, **26**, 17369-17374.
- 410 13. X. Dong, E. McCoy, M. Zhang and L. Yang, *J. Environ. Sci.*, 2014, **26**, 2526-2534.
- 411 14. A. Lovo de Carvalho, B. F. Ferreira, C. H. G. Martins, E. J. Nassar, S. Nakagaki, G. S.
412 Machado, V. Rives, R. Trujillano, M. A. Vicente, A. Gil, S. A. Korili, E. H. de Faria and
413 K. J. Ciuffi, *J. Phys. Chem. C*, 2014, **118**, 24562-24574.
- 414 15. M. R. Hoffmann, S. T. Martin, W. Choi and D. W. Bahnemann, *Chem. Rev.*, 1995, **95**,
415 69-96.
- 416 16. K. Page, M. Wilson and I. P. Parkin, *J. Mater. Chem.*, 2009, **19**, 3819-3831.
- 417 17. F. Dong, Z. Zhao, Y. Sun, Y. Zhang, S. Yan and Z. Wu, *Environ. Sci. Technol.*, 2015, **49**,
418 12432-12440.
- 419 18. N. Tian, H. Huang, C. Liu, F. Dong, T. Zhang, X. Du, S. Yu and Y. Zhang, *J. Mater.*
420 *Chem. A*, 2015, **3**, 17120-17129.
- 421 19. J. Wen, X. Li, H. Li, S. Ma, K. He, Y. Xu, Y. Fang, W. Liu and Q. Gao, *Appl. Surf. Sci.*,
422 2015, **358**, Part A, 204-212.
- 423 20. Z. Zhao, Y. Sun and F. Dong, *Nanoscale*, 2015, **7**, 15-37.
- 424 21. Y. Shiraishi, S. Kanazawa, Y. Sugano, D. Tsukamoto, H. Sakamoto, S. Ichikawa and T.
425 Hirai, *ACS Catal.*, 2014, **4**, 774-780.
- 426 22. S. C. Yan, Z. S. Li and Z. G. Zou, *Langmuir*, 2009, **25**, 10397-10401.
- 427 23. Y. Tian, B. Chang, J. Lu, J. Fu, F. Xi and X. Dong, *ACS Appl. Mater. Inter.*, 2013, **5**,
428 7079-7085.
- 429 24. J. Zhu, P. Xiao, H. Li and S. A. C. Carabineiro, *ACS Appl. Mater. Inter.*, 2014, **6**, 16449-
430 16465.
- 431 25. S. Zhang, J. Li, M. Zeng, G. Zhao, J. Xu, W. Hu and X. Wang, *ACS Appl. Mater. Inter.*,
432 2013, **5**, 12735-12743.
- 433 26. W. Wang, J. C. Yu, D. Xia, P. K. Wong and Y. Li, *Environ. Sci. Technol.*, 2013, **47**,
434 8724-8732.
- 435 27. Y. Li, L. Fang, R. Jin, Y. Yang, X. Fang, Y. Xing and S. Song, *Nanoscale*, 2015, **7**, 758-
436 764.
- 437 28. J. Huang, W. Hoc and X. Wang, *Chem. Comm.*, 2014, **50**, 4338-4340.

- 438 29. H. Zhao, H. Yu, X. Quan, S. Chen, Y. Zhang, H. Zhao and H. Wang, *Appl. Catal. B-Environ.*, 2014, **152-153**, 46-50.
- 440 30. J. Liu, T. Zhang, Z. Wang, G. Dawson and W. Chen, *J. Mater. Chem.*, 2011, **21**.
- 441 31. S. Yang, Y. Gong, J. Zhang, L. Zhan, L. Ma, Z. Fang, R. Vajtai, X. Wang and P. M. Ajayan, *Adv. Mater.*, 2013, **25**, 2452-2456.
- 442 32. P. Kubelka and F. Munk, *Z. Tech. Phys.*, 1931, **12**, 593-601.
- 443 33. J. Shi, L. Ma, P. Wu, Z. Zhou, J. Jiang, X. Wan, D. Jing and L. Guo, *ChemCatChem*, 2012, **4**, 1389-1396.
- 444 34. Y. Manevich, K. D. Held and J. E. Biaglow, *Radiat. Res.*, 1997, **148**, 580-591.
- 445 35. M.-S. Wong, D.-S. Sun and H.-H. Chang, *PLoS ONE*, 2010, **5**, e10394.
- 446 36. W. A. Rutala, E. B. Katz, R. J. Sherertz and F. A. Sarubbi, *J. Clin. Microbiol.*, 1983, **18**, 683-688.
- 447 37. D. Mulvey, P. Redding, C. Robertson, C. Woodall, P. Kingsmore, D. Bedwell and S. J. Dancer, *J. Hosp. Infect.*, 2011, **77**, 25-30.
- 448 38. N. Boonprakob, N. Wetchakun, S. Phanichphant, D. Waxler, P. Sherrell, A. Nattestad, J. Chen and B. Inceesungvorn, *J Colloid Interf. Sci*, 2014, **417**, 402-409.
- 449 39. X. Bai, L. Wang, R. Zong and Y. Zhu, *J. Phys. Chem. C*, 2013, **117**, 9952-9961.
- 450 40. F. Yang, V. Kuznietsov, M. Lublow, C. Merschjann, A. Steigert, J. Klaer, A. Thomase and T. Schedel-Niedriga, *J. Mater. Sci. A*, 2013, **1**, 6407-6415.
- 451 41. Y. L. Khung, S. H. Ngalm, A. Scaccabarozzi and D. Narducci, *Beilstein J Nanotechnol*, 2015, **6**, 19-26.
- 452 42. G. Dong, Y. Zhang, Q. Pan and J. Qiu, *J. Photoch. Photobio. C.*, 2014, **20**, 33-50.
- 453 43. X. Wang, K. Maeda, A. Thomas, K. Takanabe, G. Xin, J. M. Carlsson, K. Domen and M. Antonietti, *Nat Mater*, 2009, **8**, 76-80.
- 454 44. K. Datta, S. Sinha and P. Chattopadhyay, *Natl. Med. J. India*, 2000, **13**, 304-310.
- 455 45. P. M. Wood, *Biochem J.*, 1988, **253**, 287-289.
- 456 46. E. Cabiscol, J. Tamarit and J. Ros, *Int. Microbiol.*, 2000, **3**, 3-8.
- 457 47. J. Zhang, Y. Hu, X. Jiang, S. Chen, S. Meng and X. Fu, *J Hazard Mater*, 2014, **280**, 713-722.
- 458 48. Q. Xiang, J. Yu and P. K. Wong, *J. Colloid Interf. Sci*, 2011, **357**, 163-167.
- 459 49. X. Zhang, H. Cui, M. Humayun, Y. Qu, N. Fan, X. Sun and L. Jing, *Sci. Rep.*, 2016, **6**, 21430.
- 460 50. J. C. Yu, W. Ho, J. Lin, H. Yip and P. K. Wong, *Environ. Sci. Technol.*, 2003, **37**, 2296-2301.
- 461 51. P. S. M. Dunlop, C. P. Sheeran, J. A. Byrne, M. A. S. McMahon, M. A. Boyle and K. G. McGuigan, *J. Photoch. Photobio. A.*, 2010, **216**, 303-310.
- 462 52. A. Erkan, U. Bakir and G. Karakas, *J Photoch. Photobio. A*, 2006, **184**, 313-321.
- 463 53. M. Wakamura, K. Hashimoto and T. Watanabe, *Langmuir*, 2003, **19**, 3428-3431.
- 464
- 465
- 466
- 467
- 468
- 469
- 470
- 471
- 472
- 473
- 474
- 475
- 476



Nanostructured $g\text{-C}_3\text{N}_4$ effectively kills samples of the clinically relevant microorganisms *E. coli* O157:H7 and *S. aureus* under visible radiation.